Boundary-Layer Pitot and Hot-Wire Surveys at $M_\infty \approx 20$

M. C. Fischer,* D. V. Maddalon,† L. M. Weinstein,* and R. D. Wagner Jr.*
NASA Langley Research Center, Hampton, Va.

To examine the structure of hypersonic turbulent boundary layers, extensive boundary-layer Pitot surveys, including preliminary hot-wire, wall pressure fluctuation, and boundary-layer static pressure measurements, were obtained on the Langley Mach number 20, 22-in. helium tunnel nozzle wall. Examination of these data indicate that the boundary layer varied from nearly laminar to fully turbulent for the test range of unit Reynolds number from 0.051 to 1.41 $\times 10^6$/in. (Re_θ from 0.084 to 0.946 $\times 10^4$) with the nozzle wall temperature approximately equal to the freestream total temperature. Measured turbulent velocity profiles along the nozzle wall were fuller in the near-wall region than profiles predicted by a nonsimilar finite difference computation method. Preliminary measurements obtained with a constant current hot-wire anemometer and interpreted according to the usual linearized theory indicate mass flow fluctuations as large as 50% and total temperature fluctuations of 5% in the inner portion of the turbulent boundary layer. Static pressure increased rapidly near the wall to a level approximately 40% above the value at the boundary-layer edge. A preliminary root-mean-square wall pressure fluctuation measurement was consistent with existing lower Mach number data.

Nomenclature

A = damping function [Eq. (6) of Ref. 11]
e = voltage fluctuation across hot wire, mv
Δe_m = mass flow sensitivity
Δe_t = stagnation temperature sensitivity
l = mixing length
M = Mach number
m = ρu, lbm/ft²-sec
P = pressure, psia
Pr_t = turbulent Prandtl number
Re = Reynolds number
Re/in. = unit Reynolds number
Re_θ = Reynolds number based on momentum thickness
R_{mt} = correlation of mass flow and total temperature fluctuations
r = sensitivity ratio, $\Delta e_m/\Delta e_t$
r_w = local nozzle wall radius, in.
T = temperature, °R
u = streamwise velocity, fps
V = mean hot-wire voltage, mv
v = normal velocity, fps
x = distance from tunnel throat along nozzle wall, in.
y = perpendicular distance from wall, in.
γ = ratio of specific heats
δ = boundary-layer thickness, in.

$$\delta_{FP}^* = \int_0^\infty \left(1 - \frac{\rho u}{\rho_e u_e}\right) dy$$

$$\delta_{TC}^* = \int_0^\infty \left(1 - \frac{y}{r_w}\cos\phi\right)\left(1 - \frac{\rho u}{\rho_e u_e}\right) dy$$

$$\theta_{FP} = \int_0^\infty \frac{\rho u}{\rho_e u_e}\left(1 - \frac{u}{u_e}\right) dy$$

$$\theta_{TC} = \int_0^\infty \left(1 - \frac{y}{r_w}\cos\phi\right)\frac{\rho u}{\rho_e u_e}\left(1 - \frac{u}{u_e}\right) dy$$

ρ = density, lbm/ft³
ϕ = local slope of tunnel wall, deg

Subscripts

2 = behind normal shock
e = boundary-layer edge
l = local value
t = total
w = wall
∞ = freestream, ahead of shock

Superscripts

$\sim$ = root-mean-square
$-,\langle\ \rangle$ = time average value
prime = instantaneous value

Presented as Paper 70-746 at the AIAA 3rd Fluid and Plasma Dynamics Conference, Los Angeles, Calif., June 29–July 1, 1970; submitted August 3, 1970; revision received November 23, 1970. The authors would like to express their appreciation to D. M. Bushnell for stimulating discussions during this investigation.

* Aerospace Engineer, Viscous Flow Section, Hypersonic Vehicles Division.

† Aerospace Engineer, Space Systems Division. Associate Member AIAA.

I. Introduction

In order to predict aerodynamic friction drag and heat transfer on hypersonic flight vehicles, some understanding of the structure of the hypersonic turbulent boundary layer is necessary. A need exists for experimental hypersonic turbulent boundary-layer data to 1) provide test cases for the nonsimilar computation methods, 2) aid in developing models for the turbulent shear and heat-transfer terms in the mean flow equations, and 3) increase our understanding of turbulent flows with large density fluctuations. At the present time, only a limited number of turbulent boundary-layer surveys are available for local Mach numbers above 15 (e.g., Refs. 1 and 2) and no quantitative measurements of fluctuating properties in hypersonic turbulent boundary layers currently exist for Mach numbers above 9.[3]

In the present study, a comprehensive set of boundary-layer surveys was obtained at five locations on the wall of a contoured nozzle in helium at a nominal Mach number of 20 and $T_w/T_{t,\infty} \approx 1.0$ for a range of freestream unit Reynolds number from 0.051 $\times 10^6$ to 1.412 $\times 10^6$/in. Preliminary measurements of static pressure through the turbulent boundary layer and root-mean-square (rms) wall pressure fluctuations were also obtained. In addition, preliminary measurements of fluctuating mass flow and total temperature were obtained with a constant current hot-wire anemometer.

II. Test Facility, Procedures, Instrumentation, and Corrections to Pitot Data

Test Facility

The present experimental investigation was conducted in the Langley $M \approx 20$ 22-in. hypersonic helium tunnel, which has an axisymmetric contoured nozzle. The test-section diameter is 22 in. and the freestream Mach number varies with stagnation pressure from 16.1 at 75 psia to 22.3 at 3015

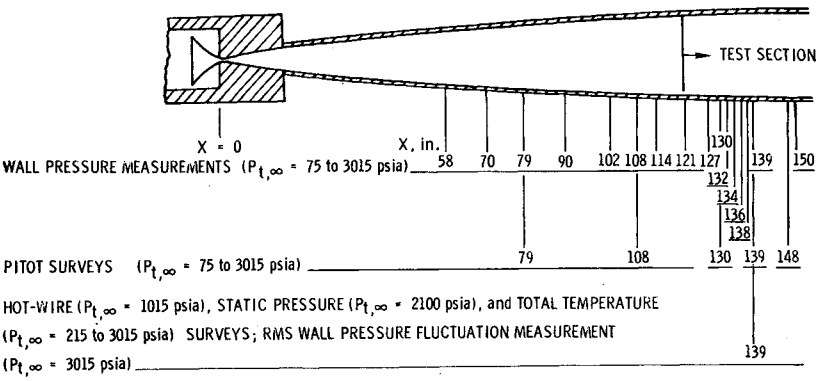

Fig. 1 Measuring stations along nozzle wall.

psia. A detailed description and calibration of the facility is presented in Ref. 4.

Test Procedures and Instrumentation

Pitot pressure surveys through the boundary layer were obtained in unheated flow at the five nozzle wall locations indicated on Fig. 1. Comprehensive Pitot surveys in the center of the test section (station 139) were made with a single traversing probe, 0.125-in. in diameter and 0.013-in. wall thickness, for a range of stagnation pressures from 75 psia to 3015 psia. A sketch of the probe is shown in Fig. 2a.

Because of access problems, Pitot surveys could not easily be obtained at other nozzle stations with the single traversing probe. Therefore, a Pitot rake (Fig. 2b) was used to obtain Pitot pressure surveys at station 79 for stagnation pressures of 515, 1015, and 2065 psia. The same rake was used to obtain Pitot pressure surveys at stations 108, 130, and 148 for a stagnation pressure of about 2000 psia.

Measurements of static pressure through the boundary layer at station 139 were made at a stagnation pressure of 2100 psia with the static pressure rake shown in Fig. 2c. The rake contained two static pressure probes and remained stationary for each run. The probes were constructed of 0.125-in.-diam (0.018-in. wall thickness) stainless-steel tubing with a 42.5° half-angle conical tip. Four equally spaced (90° apart) orifice holes, 0.030 in. in diameter, were located approximately 3.6 tube diameters downstream of the sharp tip. Probes of this type provide a fairly accurate measurement of static pressure using blast wave or characteristics theory.[5] Wall static pressures were measured at 16 locations along the tunnel nozzle, as indicated on Fig. 1.

A preliminary measurement of rms wall pressure fluctuation was obtained at $P_{t,\infty} = 3015$ psia, using a Kistler model 606L pressure pickup transducer which has a diameter of 0.436 in. and is capable of recording pressures up to 30 psia. Resonant frequency for this transducer is 140 kHz. The transducer was mounted flush with the wall of the test section, and a Kistler model 818 accelerometer, with a range of $250g$, mounted in the tunnel wall, recorded the noise level due to tunnel vibration. This background noise as well as electronic noise was subtracted from the measured wall surface fluctuating pressure level to correct the reading of rms wall pressure fluctuation. The low pass filter was set at 50 kHz so that the wall pressure fluctuation measurement frequency range was 5–50,000 Hz.

Stagnation temperatures were measured with shielded tungsten resistance thermometer total temperature probes.

Experimental hot-wire techniques developed by Wagner and Weinstein[6] were used in the present study to obtain mass flow and total temperature fluctuation data. A constant current hot-wire probe was set in one position during a given run. About six overheats were used to obtain sufficient redundant data for deducing $\tilde{T}_t$, $\tilde{m}$, and R_{mt} using the Kovasznay mode diagram method.[7] A range of y = 2–10 in. was examined using the hot wire. The hot-wire tests were all conducted at station 139 with $P_{t,\infty} \approx 1000$ psia ($\delta \approx 7.0$ in.).

Corrections to Pitot Data

The Pitot pressure measurements were corrected for both real gas, viscous interaction, and rarefaction effects. In addition, a turbulence correction was calculated and applied to the Pitot data to estimate the maximum effect on the profiles.

Real-gas corrections were applied using the results of Ref. 8 and were greatest at the higher stagnation pressures. For any individual run, the Pitot data in the outer portion of the boundary layer (higher local Mach number) received the greatest correction. Conversely, viscous and rarefaction effects become significant at the small local Reynolds number conditions typical of the inner portion of the boundary layer. Corrections to the Pitot data for viscous interaction and rarefaction effects were made using results of an unpublished study by Harvey and Clark at Langley, and the results of Rogers et al.[9] The size of the correction depends primarily on the magnitude of M_ℓ and $Re_{\ell,d}$, where $Re_{\ell,d}$ is the local Reynolds number based on Pitot probe diameter. The maximum viscous and rarefaction correction for this investigation was about 20% (reduction in $P_{t,2}$) and occurred for the measurements nearest the wall. At the higher total pressures ($P_{t,\infty} \geq 1000$ psia), only the first few measurements near the wall (low local Reynolds and Mach numbers) received a significant correction.

An estimate was made of the maximum error in the Pitot pressure measurements due to the effects of turbulence.

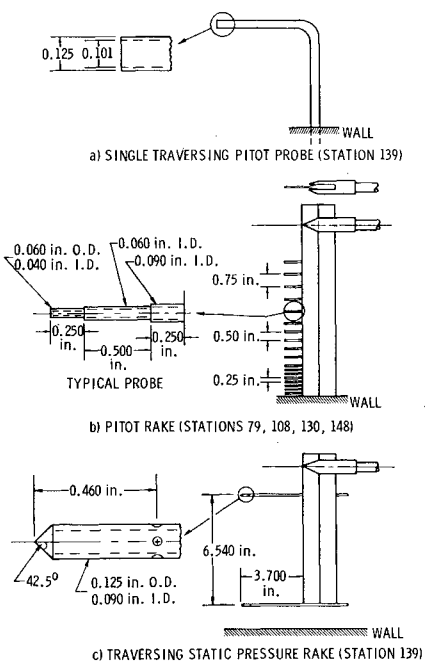

Fig. 2 Pitot and static pressure survey apparatus.

Table 1. Summary of tunnel wall boundary-layer Pitot surveys with $T_w/T_{t,\infty} \approx 1.0$ ($T_{t,\infty} \approx 540°$ R)

Station	M_e	$P_{t,\infty}$, psia	Re_∞/in. $\times 10^{-6}$	$Re_{\theta TC}$, $\times 10^{-4}$	δ_{FP}^*, in.	δ_{TC}^*, in.	θ_{FP}, in.	θ_{TC}, in.	δ, in.
79	17.7	515	0.327	0.252	2.07	2.01	0.0091	0.0077	3.8
79	18.4	1015	0.655	0.412	1.77	1.73	0.0072	0.0063	3.4
79[a]	19.0	2065	1.261	0.606	1.42	1.39	0.0055	0.0048	3.1
108[a]	20.8	2065	1.151	0.680	2.17	2.10	0.0070	0.0059	4.4
130[a]	21.6	2065	1.100	0.759	2.72	2.62	0.0082	0.0069	5.9
139	16.1	75	0.051	0.084	5.44	5.31	0.0239	0.0165	8.3
...	16.9	120	0.079	0.134	5.88	5.73	0.0251	0.0169	8.2
...	17.1	165	0.108	0.171	5.29	5.10	0.0226	0.0158	7.9
...	17.5	225	0.146	0.223	5.18	4.95	0.0217	0.0153	7.9
...	17.9	275	0.171	0.246	4.96	4.81	0.0200	0.0144	8.0
...	18.2	315	0.194	0.266	4.82	4.61	0.0190	0.0137	8.0
...	18.6	365	0.220	0.286	4.69	4.49	0.0177	0.0130	7.5
...	18.7	415	0.248	0.322	4.57	4.42	0.0174	0.0130	7.5
...	18.8	465	0.278	0.353	4.54	4.30	0.0172	0.0127	7.5
...	19.1	515	0.302	0.362	4.27	4.09	0.0158	0.0120	7.4
...	19.4	615	0.305	0.339	3.99	3.83	0.0144	0.0111	7.0
...	20.0	765	0.423	0.453	3.90	3.73	0.0137	0.0107	6.6
...	20.4	1015	0.548	0.537	3.70	3.53	0.0125	0.0098	6.8
...[a]	21.6	2015	1.010	0.707	2.78	2.71	0.0083	0.0070	6.0
...	22.3	3015	1.412	0.946	2.74	2.67	0.0079	0.0067	5.5
148[a]	21.5	2055	1.102	0.915	3.38	3.22	0.0103	0.0083	7.4

[a] Reduced assuming variable static pressure.

The basic Pitot equation can be expressed as[3]

$$P_{t,2} = G(M)\rho u^2 \quad (1)$$

where $G(M)$ is a slowly varying function of Mach number for $M \gtrsim 2$. Substituting into the Pitot equation the conventional mean and fluctuating terms and expanding, one obtains an expression for the mean Pitot reading in terms of the fluctuating velocity and density. Substituting into this equation estimates of the peak velocity and density fluctuations, which occur at about $y/\delta \approx 0.1$, and assuming the correlation coefficient between velocity and density is $+1.0$, one finds that the mean measured Pitot value could be 24% higher than the true value. However, this "extreme case" correction would reduce the velocity profile by an insignificant amount. Because of the uncertainty in its magnitude and the fairly small effect on u/u_e, the turbulence correction was not used to reduce the profiles discussed in the present report.

Profiles were calculated from the corrected Pitot data assuming constant static pressure through the boundary layer except for the test runs obtained at $P_{t,\infty} \approx 2000$ psia for the five nozzle wall locations. Static pressure measurements through the boundary layer in the test section at $P_{t,\infty} \approx 2000$ psia indicated an increase in static pressure near the wall (this result will be discussed more fully in a later section of the present paper). This increase was verified from mean wall static pressure measurements and occurred when the wall boundary layer was turbulent. However, since the actual manner in which the static pressure varied with y was measured at $P_{t,\infty} \approx 2000$ psia only, the five $P_{t,\infty} \approx 2000$ psia surveys were reduced assuming a variable static pressure distribution similar to that measured [i.e., $\bar{P}/\bar{P}_e = f(y/\delta)$ based on station 139 measurements].

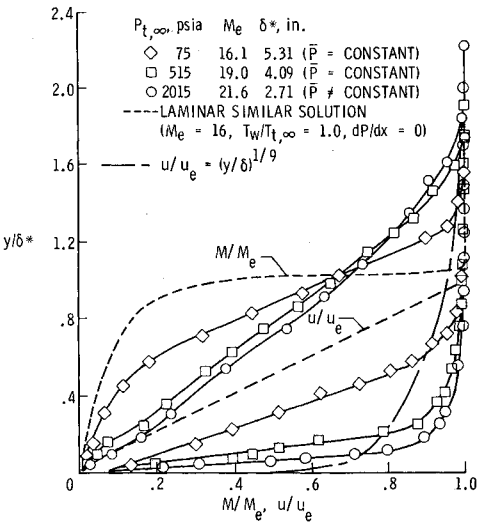

Fig. 3 Nozzle wall boundary-layer profiles at station 139.

III. Results and Discussion

Pitot Surveys

Mach number profiles were calculated from the corrected Pitot pressures (corrected for real gas, viscous interaction, and rarefied flow effects), assuming constant static pressure through the boundary layer except for the five test runs obtained at $P_{t,\infty} \approx 2000$ psia. As discussed previously, these five Pitot surveys were reduced assuming a variable static pressure through the boundary layer. Velocity and density profiles were computed using a constant total temperature through the boundary layer. This assumption was considered valid since total temperature measurements through the boundary layer indicated small deviations from the freestream total temperature. Table 1 summarizes the conditions for the Pitot surveys and contains calculated displacement thickness and momentum thickness values both with (subscript TC) and without (subscript FP) a transverse curvature correction (see Nomenclature). The edge of the boundary layer was taken as the point of maximum Pitot pressure ($dP_{t,2}/dy = 0$). Table 2 presents the data from the 2000 psia surveys at four nozzle locations in tabulated form and also includes the uncorrected pitot data.

The results of Pitot surveys obtained at station 79 for $P_{t,\infty} = 515$ and 2065 psia indicate a turbulent boundary layer at both stagnation pressures, with the profile fullness increasing with stagnation pressure. Profiles computed from Pitot surveys at stations 108 and 130 for $P_{t,\infty} = 2065$ psia also indicated turbulent flow.

A comprehensive set of boundary-layer surveys was obtained at station 139 (center of test section) for a range of tunnel stagnation pressure from 75 psia to 3015 psia (see Table 1). Representative profiles are shown in Fig. 3 along with a theoretical laminar similar solution.[10] At the lowest

Table 2 Tabulated profile data for the four $P_{t,\infty}$ = 2000 psia nozzle wall stations

Station 79, $P_{t,\infty}$ = 2065 psia, $T_{t,\infty}$ = 540°R, δ_{TC}^* = 1.39 in., $P \neq C$			Station 108, $P_{t,\infty}$ = 2065 psia, $T_{t,\infty}$ = 540°R, δ_{TC}^* = 2.10 in., $P \neq C$			Station 130, $P_{t,\infty}$ = 2065 psia, $T_{t,\infty}$ = 540°R, δ_{TC}^* = 2.62 in., $P \neq C$			Station 139, $P_{t,\infty}$ = 2015 pia, $T_{t,\infty}$ = 540°R, δ_{TC}^* = 2.71 in., $P \neq C$		
y, in.	M/M_e	u/u_e	y, in.	M/M_e	u/u_e	y, in.	M/M_e	u/u_e	y, in.	M/M_e	u/u_e
0.000	0.000	0.000	0.000	0.000	0.000	0.000	0.000	0.000	0.000	0.000	0.000
0.070	0.030	0.318	0.070	0.026	0.303	0.070	0.016	0.204	0.070	0.017	0.215
0.150	0.112	0.780	0.200	0.059	0.584	0.200	0.060	0.602	0.130	0.025	0.308
0.298	0.223	0.929	0.298	0.087	0.725	0.298	0.119	0.832	0.160	0.044	0.490
0.533	0.314	0.964	0.400	0.193	0.921	0.400	0.176	0.913	0.210	0.056	0.580
0.777	0.393	0.978	0.533	0.250	0.952	0.533	0.221	0.943	0.270	0.081	0.713
1.028	0.535	0.989	0.777	0.300	0.967	0.777	0.270	0.961	0.320	0.105	0.797
1.297	0.666	0.994	1.028	0.370	0.979	1.028	0.301	0.969	0.490	0.157	0.894
1.562	0.756	0.996	1.297	0.462	0.987	1.297	0.364	0.979	0.670	0.204	0.933
1.830	0.837	0.998	1.562	0.587	0.993	1.562	0.444	0.987	0.830	0.234	0.949
2.293	0.950	0.999	1.830	0.636	0.994	2.293	0.639	0.995	1.470	0.372	0.980
2.803	1.020	1.000	2.293	0.734	0.997	2.803	0.717	0.997	2.010	0.534	0.992
3.325	1.000	1.000	2.803	0.820	0.998	3.325	0.811	0.998	2.470	0.631	0.995
3.825	1.021	1.000	3.325	0.925	0.999	3.825	0.881	0.999	2.930	0.733	0.997
4.355	1.051	1.000	3.825	0.983	0.999	4.355	0.951	0.999	3.660	0.858	0.998
5.100	1.087	1.000	4.355	0.999	0.999	5.100	0.994	0.999	4.100	0.902	0.999
5.860	1.124	1.000	5.100	1.007	1.000	5.860	1.000	1.000	4.360	0.953	0.999
6.592	1.157	1.001	5.860	1.023	1.000	6.592	1.003	1.000	4.980	0.991	0.999
			6.592	1.038	1.000	7.330	0.986	0.999	5.380	0.994	0.999
			7.330	1.030	1.000	8.110	1.000	1.000	6.000	1.000	1.000
			8.110	1.039	1.000				7.100	1.011	1.000

Uncorrected Pitot data

Station 79		Station 108		Station 130		Station 139	
y, in.	$P_{t,2}$, psia	y, in.	$P_{t,2}$, psia	y, in.	$P_{t,2}$, psia	y, in.	$P_{t,2}$, psia
0.000	0.021	0.000	0.012	0.000	0.010	0.000	0.009
0.070	0.026	0.070	0.017	0.070	0.014	0.070	0.012
0.298	0.447	0.298	0.060	0.298	0.089	0.130	0.013
0.533	0.881	0.533	0.465	0.533	0.298	0.160	0.017
0.777	1.159	0.777	0.671	0.777	0.448	0.210	0.024
1.028	1.738	1.028	0.825	1.028	0.554	0.270	0.043
1.297	2.469	1.297	1.068	1.297	0.723	0.320	0.067
1.562	3.310	1.562	1.437	1.562	0.932	0.490	0.148
1.830	4.187	1.830	1.745	2.293	1.556	0.670	0.245
2.293	5.681	2.293	2.411	2.803	2.010	0.830	0.326
2.803	7.066	2.803	3.164	3.325	2.703	1.470	0.680
3.325	7.105	3.325	4.228	3.825	3.302	2.010	1.050
3.825	6.744	3.825	5.009	4.355	3.985	2.470	1.500
4.355	6.159	4.355	5.453	5.100	4.593	2.930	2.100
5.100	5.558	5.100	5.347	5.860	4.886	3.660	3.010
5.860	5.038	5.860	5.102	6.592	4.818	4.100	3.420
6.592	4.609	6.592	4.882	7.330	5.093	4.360	3.900
		7.330	4.985	8.110	4.895	4.980	4.400
		8.110	4.908			5.380	4.520
						6.000	4.780
						7.100	4.600

pressure, the velocity profile appeared to be nearly laminar when compared with the laminar similar solution result. The higher pressure velocity profiles are fuller than a $\frac{1}{9}$-power law (typical turbulent) profile. Profiles obtained at the last survey station (station 148) for $P_{t,\infty}$ = 2055 psia were believed affected by the upstream influence of the adverse pressure gradient flow in the diffuser section and are therefore not shown.

Comparison of Measured and Predicted Profiles

Measurement of the turbulent Pitot profiles along the tunnel wall at $P_{t,\infty} \approx 2000$ psia provides a test case for the developing nonsimilar computation methods that can compute the downstream development of a turbulent boundary-layer flow with a known upstream profile as an input. The nonsimilar finite difference computation method of Bushnell and Beckwith[11] was used for the present study to indicate typical results using one of the presently available methods as applied to a $M \approx 20$ adiabatic helium flow. In this method, the Reynolds stress is modeled by an eddy viscosity function with a mixing length that is dependent on the distance from the wall and the boundary-layer thickness. In the near-wall region, Van Driest's exponential damping function is used. The velocity profile at station 79 was inputed along with the velocity, density, Mach number, and velocity gradient at the boundary-layer edge (see Table 3 for complete list of inputs used). Four cases were computed using the computation method[11]: 1) a turbulent Prandtl number of $Pr_t = 1$ and mixing length parameter of $(l/\delta)_{max} = 0.09$ were used, with the damping function [A term in Eq. (6) of Ref. 11] evaluated at the wall; 2) the turbulent Prandtl number was equal to 1, but the eddy viscosity model was altered so that the damping function A was evaluated as a function of distance from the wall; 3) same as case 2 but with $Pr_t = 0.6$ for $y/\delta > 0.2$, going to $Pr_t = 1$ at wall; and 4) same as case 2 but with $(l/\delta)_{max} = 0.12$. Comparisons of the measured and predicted velocity profiles are presented in Fig. 4 for stations 108, 130, and 139. Solutions from the four cases of the computation method are shown as a shaded band. The experimental displacement thickness (δ_{exp}^*) with transverse curvature was

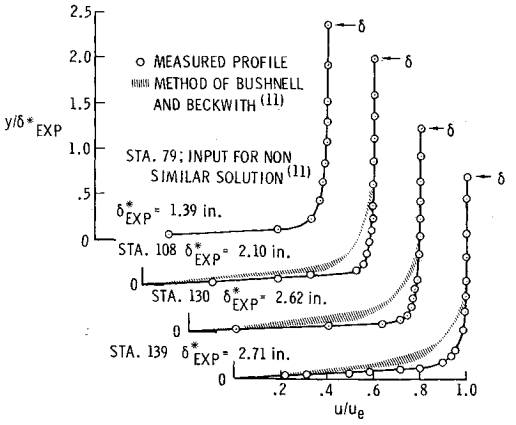

Fig. 4 Comparison of measured and predicted velocity profiles.

used to normalize both experimental and predicted results. It is apparent that the measured velocity profiles were fuller than the nonsimilar method predictions in the inner portion of the boundary layer. The case with $Pr_t = 1.0$, $(l/\delta)_{max} = 0.12$, and a damping function that was evaluated as a function of y gave the best agreement with measured velocity slopes near the wall, but also gave the poorest agreement for $y/\delta^* \geq 0.4$. A recent analysis of the profiles presented herein by D. M. Bushnell of Langley indicates that the slope of mixing length with y near the wall is approximately 0.6 as opposed to the value 0.4 used in the calculations shown on Fig. 4. Theoretical calculations using this 0.6 slope, $(l/\delta)_{max} = 0.18$, and the damping function evaluated at the wall (using the method of Ref. 11) gave much better agreement with the experimental profiles. Therefore, since higher values of mixing length wall slope are typical of low Reynolds number turbulent flows, it is suggested that the factor of 150 change in density across the present Mach 20 boundary layer causes the wall region to behave in a similar fashion to a low-speed, low Reynolds number turbulent boundary-layer flow. It should be noted that both data and theory indicate a very high N power for the outer portion of the boundary layer. The excessive fullness of the velocity profiles when compared to nonsimilar computation method results was also shown by Herring and Mellor[12] at $M_e = 1.9$–4.9 on a nozzle wall. As in the present case, Herring and Mellor improved the agreement between predicted and measured velocity profiles by modifying the eddy viscosity model. For the present case, there are other probable reasons for the disagreement in predicted and measured velocity profiles. All of the measured

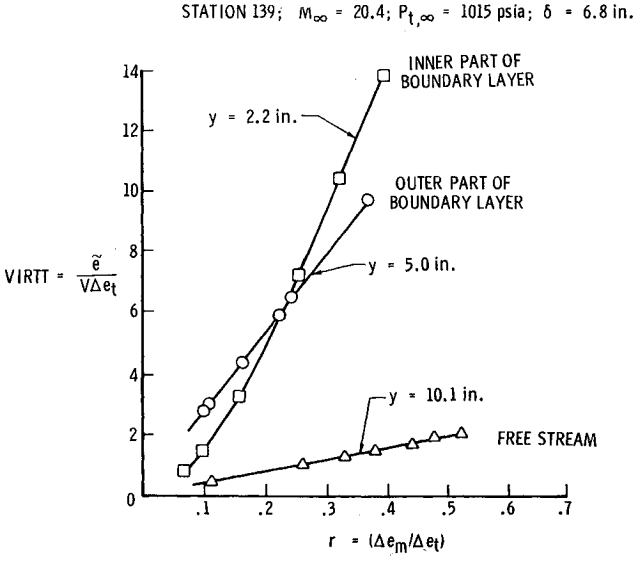

Fig. 5 Variation of virtual total temperature fluctuation with sensitivity ratio.

profiles shown in Fig. 4 were reduced with a variable static pressure through the boundary layer, whereas the nonsimilar solution method utilized the usual boundary-layer assumption of constant static pressure. In addition, the computation method does not include transverse curvature effects, which may be a significant contribution for these conditions. Also, the computation method does not include density fluctuation terms in the eddy viscosity model. These density fluctuation terms may be large for hypersonic turbulent boundary layers with large density ratios across the boundary layer.[11] Another possibility is that the Pitot pressure measurements near the wall are in error. Wallace[13] reported Pitot fluctuations as large as 50% near the wall at $M_\infty = 8$. Pitot fluctuations of this magnitude or larger probably occurred near the wall in the present study. These fluctuations could cause the mean pressure sensed at the measuring end of the Pitot tube to be above the true mean, since the measuring system will probably favor the high peaks rather than the lower valleys of a fluctuating pressure. In addition, the static pressure distribution in the boundary layer may be more extreme than the distribution used. Also, probe interference with the wall may have distorted the local flow conditions. However, wall static pressure measurements in the proximity of the probe indicated no irregularities in the wall static pressure level.

Although the various reasons postulated for the disagreement between measured and predicted profiles in Fig. 4 should be investigated be ore definite conclusions can be made, the evidence tends to indicate that the excessive measured velocity profile fullness in the lower part of the boundary layer ($y/\delta^* \approx 0.3$) may be due to the large eddy viscosity values associated with the low Reynolds number turbulent flow in the inner portion of the present boundary layer (region of low density).

Hot-Wire Fluctuation Measurements

Since a hot wire essentially responds to mass flow and total temperature fluctuations, a modal analysis of rms mass flow and total temperature fluctuations can be made as suggested in Ref. 7. The assumption of small disturbance levels was made in Ref. 7 to simplify the equations, but the present results tend to indicate that fairly high disturbance levels were, in fact, encountered. In addition, the hot-wire system used (constant current) tends to be highly nonlinear for large disturbance levels primarily due to incorrect compensation. The effect of the last two failings has not been examined herein and, therefore, the results presented must be viewed cautiously as indicating trends rather than absolute magnitudes.

The calibration techniques, data reduction procedures, and the complete hot-wire system used are described in Ref. 6. The data analysis is based on the Kovasznay[7] approach, for which the virtual total temperature fluctuation, $\tilde{e}/(V\Delta e_t)$, is related to the sensitivity, $r = \Delta e_m/\Delta e_t$, by

$$\left(\frac{\tilde{e}}{V\Delta e_t}\right)^2 = \left(\frac{\tilde{T}_t}{\bar{T}_t}\right)^2 - 2r\frac{\tilde{T}_t}{\bar{T}_t}\frac{\tilde{m}}{\bar{m}}R_{mt} + r^2\left(\frac{\tilde{m}}{\bar{m}}\right)^2 \qquad (2)$$

where $R_{mt} = \langle m'T'_t\rangle/\tilde{m}\tilde{T}_t$. For each test, the hot wire is operated at several sensitivity ratios (values of current), and $\tilde{e}/(V\Delta e_t)$ is generated as a function of r. A plot of the values of $\tilde{e}/(V\Delta e_t)$ and r is faired and three points are picked off the fairing. From these points, the three coefficients, $\tilde{T}_t/\bar{T}_t$, R_{mt}, and $\tilde{m}/\bar{m}$ can be obtained. Figure 5 shows plots of Virtt

Table 3 Input for nonsimilar computation method of Bushnell and Beckwith[11]

Station, in.	Me	ρ/ρ ($\times 10^3$)	$u_e/(2H_e)^{1/2}$	r_w, in.	du_e/dx
79	19.0	0.741	0.995	8.00	0
108	20.8	0.574	...	9.30	...
130	21.6	0.511	...	10.75	...
139	21.6	0.500	...	10.95	...

$[\tilde{e}/(V\Delta e_t)]$ vs $r(\Delta e_m/\Delta e_t)$ for typical positions in and above the Mach 20 boundary layer. For $y = 10.1$ in. (in the free-stream), the intercept for $r = 0$ is small and positive and the faired curve is a straight line. These fluctuations are believed to be sound radiated by the turbulent boundary layer upstream in the nozzle.[6,14] At $y = 5.0$ in., which is in the boundary layer, the slope is much higher but is still a straight line with a slightly positive intercept for $r = 0$. In the inner portion of the boundary layer ($y = 2.2$ in.), the faired line is nonlinear for small values of r, whereas the straight portion has a negative intercept trend. The fluctuating mass flow and total temperature coefficients, $\tilde{m}/\bar{m}$ and $\tilde{T}_t/\bar{T}_t$ and the correlation coefficients R_{mt}, determined from these mode plots, are shown in Figs. 6–8. Data scatter is apparent; the mass flow fluctuations are most reliable since they are determined by the slope of the faired mode plots at large values of r which could be obtained to some accuracy. But the $\tilde{T}_t/\bar{T}_t$ and R_{mt} coefficients are determined by the details of the mode diagram near small r; this results because of the order of magnitude difference in the levels of $\tilde{m}/\bar{m}$ and $\tilde{T}_t/\bar{T}_t$. Unfortunately, the present mode diagrams do not contain sufficient data points at low sensitivity to accurately determine $\tilde{T}_t/\bar{T}_t$ or R_{mt}. Nevertheless, the trends shown in these quantities are probably reasonable. The mass flow fluctuation results (Fig. 6) indicate fluctuations as large as 50% in the inner portion of the boundary layer. This is a significant increase as compared to the maximum mass flow fluctuations of about 15% measured by Kistler[15] at $M_\infty = 4.7$ (see Fig. 6). These large fluctuations in mass flow near the wall probably represent large fluctuations in density and may be typical of hypersonic turbulent flows with large density ratios across the boundary layer ($\rho_e/\rho_w \approx 150$ for the present case). The presence of large density fluctuations indicates that more terms should be considered in the expanded Reynolds stress expression [Eq. (4) of Ref. 11];

$$\langle(\rho v)'u'\rangle = \bar{\rho}\langle v'u'\rangle + \bar{v}\langle\rho'u'\rangle + \langle\rho'v'u'\rangle \qquad (3)$$

where the last two terms are generally considered negligible. Also presented in Fig. 6 is a mean-mass-flow profile (from Pitot surveys) and an approximation of the mass flow fluctuation based on Prandtl's mixing length (after Ref. 3)

$$\tilde{m}/\bar{m}_l = (l/\delta)[d(\bar{m}_l/\bar{m}_e)/d(y/\delta)](\bar{m}_e/\bar{m}_l) \qquad (4)$$

where

$$l/\delta \approx 0.4\, y/\delta \text{ for } y/\delta \leq 0.2$$

$$l/\delta \approx 0.08 \text{ for } y/\delta \geq 0.2$$

The approximation gives good agreement with the maximum mass flow fluctuations measured. Total temperature fluctuations as large as 5% were measured in the inner portion of the boundary layer (Fig. 7). A further observation can be made concerning the measured mass flow fluctuations in the boundary layer. The mean velocity profile is essentially flat over the upper half of the boundary layer ($u/u_e = 0.995$ at $y/\delta^* \approx 1.0$) as shown in Fig. 3. Fluctuations in velocity are therefore probably negligible in the absence of any mean velocity gradient. This conclusion is further supported by the sharp decrease in the total temperature fluctuation level in the outer half of the boundary layer (Fig. 7). One can then assume that the mass flow fluctuation levels measured in the outer portion of the boundary layer ($y/\delta^* \geq 1.0$, Fig. 6) are composed mostly of pressure fluctuations (sound mode is dominant), which are attenuated in intensity with increasing distance from the sound source. The variation of the correlation coefficient through the boundary layer is shown in Fig. 8. The reversal of sign in the inner part of the boundary layer suggests that vorticity, for which $R_{mt} = +1.0$, may be the dominant disturbance mode. This result was also shown by Kistler[15] in a supersonic turbulent boundary layer.

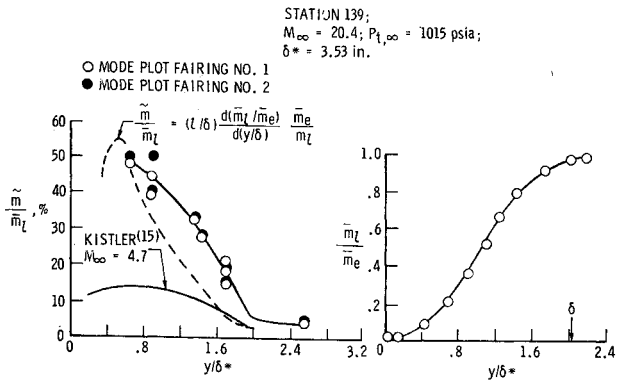

Fig. 6 Mass flow fluctuation in turbulent nozzle wall boundary layer.

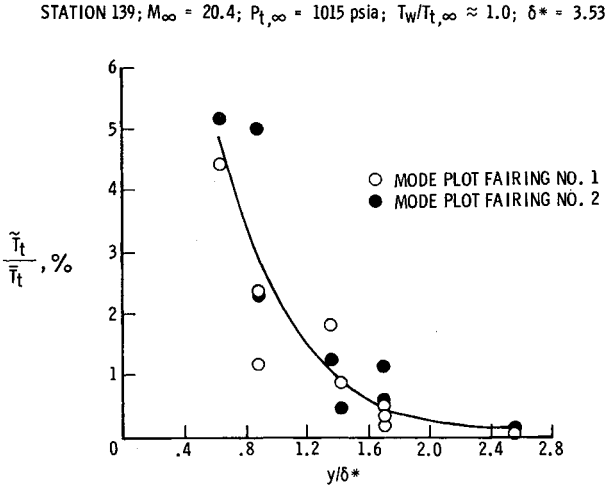

Fig. 7 Total temperature fluctuation in turbulent nozzle wall boundary layer.

Wall Static Pressure

Static pressure measurements were obtained at numerous stations along the nozzle wall (see Fig. 1). The variation of wall pressure with increasing stagnation pressure for five representative stations is shown in Fig. 9. There is a definite increase in wall pressure, with increasing stagnation pressure, starting at about $P_{t,\infty} = 450$ psia for station 139 and about $P_{t,\infty} = 600$ psia for station 79. This increase in

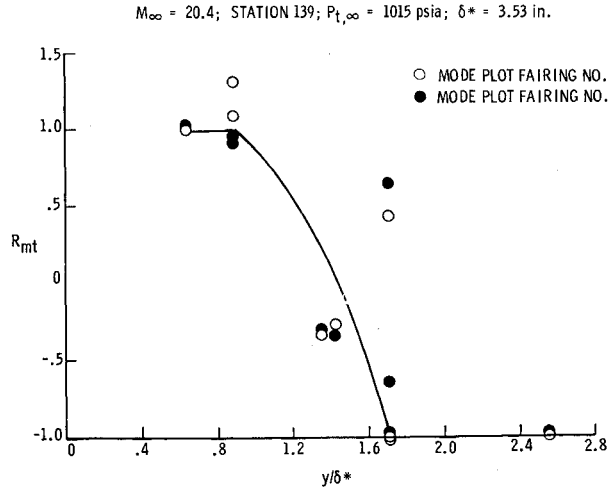

Fig. 8 Variation of mass flow—total temperature correlation coefficient through turbulent nozzle wall boundary layer.

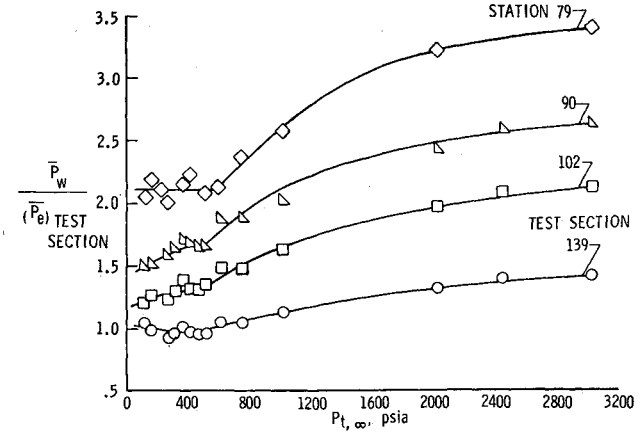

Fig. 9 Variation of mean wall static pressure with tunnel stagnation pressure.

static wall pressure could be tentatively attributed to either 1) some mechanism associated with the onset of transition and fully developed turbulent flow or 2) uncanceled Mach waves entering the boundary layer. For the first possibility, the fluctuating normal velocity v' that is present in a turbulent boundary layer could cause an increase in the mean wall pressure level at this high Mach number (i.e., the terms in the y momentum equation are no longer negligible for $dP/dx \approx 0$ and turbulent flow). Conversely, uncanceled Mach waves may be entering the boundary layer near the region surveyed, thus raising the wall static pressure level above that at the boundary-layer edge. Velocity profiles obtained at station 139 indicate a turbulent nozzle wall boundary layer at $P_{t,\infty} \approx 500$ psia (Fig. 3). Velocity profiles for station 79 indicate that the boundary layer was also turbulent for $P_{t,\infty} \approx 500$ psia. These results give credibility to the reasoning that the rise in wall static pressure is due to the presence of a transitional-turbulent boundary layer near the wall. The start of transition apparently begins in the test section for low values of total pressure (unit Reynolds number) and moves quickly up the nozzle with increasing total pressure (see Ref. 6). The significance of Fig. 9 is that there is evidently a normal pressure gradient across the present Mach 20 turbulent boundary layer. Kemp and Sreekanth[2] also noted the same effect at hypersonic Mach numbers.

An analysis was made of the possible error in measured wall static pressure due to shear effects at the wall orifice based on the study of Shaw[16] and Rainbird.[17] Specifically, Rainbird[17] shows that shear effects will increase a wall orifice pressure reading significantly only when the ratio of hole diameter to boundary-layer displacement thickness is equal to about one or greater. For the present case, d/δ^* varies

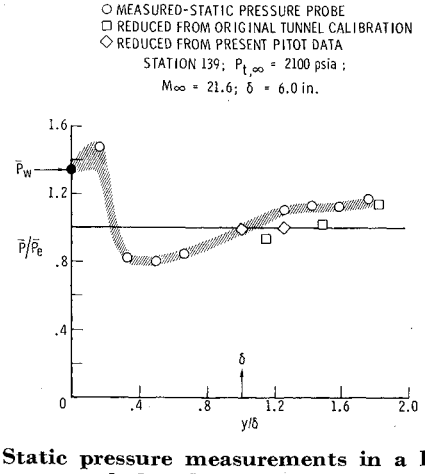

Fig. 10 Static pressure measurements in a hypersonic turbulent boundary layer.

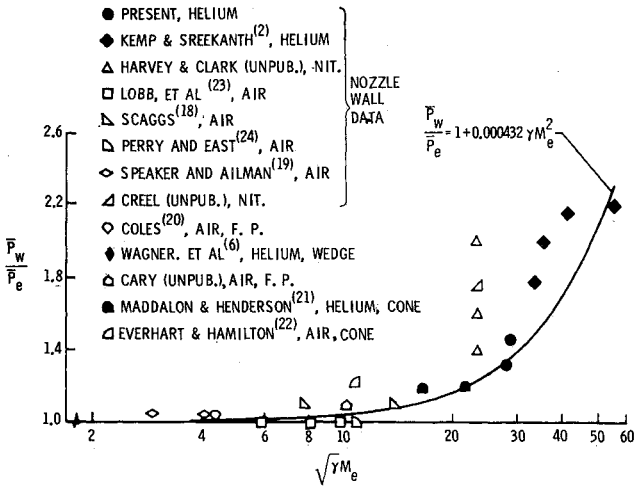

Fig. 11 Variation of wall static pressure with Mach number in a turbulent boundary layer, $dP/dx \approx 0$.

from 0.017 to 0.085 and, therefore, the effects of shear on the wall static pressure orifice are believed negligible.

Boundary-Layer Static Pressure Profile

Static pressure measurements were made through the turbulent boundary layer at station 139 and $P_{t,\infty} \approx 2100$ psia to attempt to determine if the rise in wall pressure was due to transitional-turbulent flow or if uncanceled Mach waves were responsible. A cone-cylinder characteristics solution was used with the measured probe surface pressure to obtain a local freestream static pressure. There is the question of possible viscous corrections to the measured static pressure data. From Ref. 5, conically tipped axisymmetric probes of the type used in the present investigation (with large cone half-angle) have small viscous corrections. This finding is strengthened by the fair agreement between freestream static pressure determined from the probe measurement and that calculated from the present Pitot data.

The measured static pressure through the boundary layer, nondimensionalized by the static pressure at the boundary-layer edge, is shown in Fig. 10. The measurements indicate that the static pressure decreases below the value at the boundary-layer edge in the outer part of the boundary layer and then increases to approximately 40% above the edge value near the wall. Therefore, in a hypersonic turbulent boundary layer, the assumption of constant static pressure across the boundary layer ($dP/dy = 0$) may not be valid. Only the Pitot data obtained at $P_{t,\infty} \approx 2000$ psia were reduced assuming a variable static pressure across the boundary layer. The shaded symbol at $y = 0$ (Fig. 10) represents the measured wall static pressure, which was about 35% above the static pressure at the boundary-layer edge. An increase in measured wall static pressure due to uncanceled Mach waves is thus not likely, since Mach waves entering the boundary layer would presumably have produced increases in static pressure in the outer portion of the boundary layer as opposed to the results of the present measurements which indicate an increase in the inner portion. Thus, the increase in measured wall pressure can be tentatively attributed to the presence of transitional or turbulent flow effects.

Mean and rms Wall Static Pressure

Numerous investigators have reported an increase in measured mean wall static pressure over the corresponding value at the boundary-layer edge.[2,6,18–22] The trend of these increases in $\bar{P}_w/\bar{P}_e$ with Mach number are shown in Fig. 11, along with the data of Refs. 23–24. Large increases in the mean wall static pressure level are seen to occur at high Mach

number. The solid curve that represents the general trend of the data can be expressed mathematically as

$$\tilde{P}_w/\tilde{P}_e = 1 + 0.000432\gamma M_e^2 \quad (5)$$

and was derived from application of a simplified form of the y momentum equation.

The v' normal velocity components that may contribute to the observed increase in mean wall static pressure are probably the result of large, low-frequency, large-wavelength eddies outside the laminar sublayer which dominate the pseudo-sound generation in the boundary layer. Sound that is radiated into the freestream is probably generated by intense high-frequency, short-wavelength Eddies near the edge of the laminar sublayer.[25] Measurements of the sound source velocity (u_s) obtained by Wagner et al.,[6] and also verified in the present study, indicate that the source velocity is just supersonic relative to the freestream ($u_s/u_\infty \approx 0.95$) at $M_\infty \approx 22$. Laufer[14] showed that at supersonic freestream Mach numbers ($M_\infty \approx 2$–5) the source velocity was highly supersonic relative to the freestream ($u_s/u_\infty \approx 0.3$–0.6). The intensity of the large, lower frequency eddies, which are convected at approximately $u_c \geq 0.8\, u_\infty$ (subsonic relative to the freestream) is time dependent and thus produces fluctuations ($\tilde{P}_w$) in the mean wall static pressure.

Measured values of $\tilde{P}_w$ from previous studies[19,26–29] are presented in Fig. 12 along with a preliminary measurement obtained by Stainback during the current investigation. Kistler and Laufer's results were taken from Richards et al.[26] The theories of Houbolt[30] and Lowson (as reported by Pierce and Mayes[31]) are also shown. In previous investigations, $\tilde{P}_w$ was assumed equal to $\bar{P}_e$ (constant static pressure across the boundary layer). This assumption was valid, since previous data were obtained at $M_\infty \leq 5$ where $\tilde{P}_w \approx \bar{P}_e$ (see Fig. 11). However, for higher Mach numbers $\tilde{P}_w > \bar{P}_e$ and thus the ratio $\tilde{P}_w/\bar{P}_e$ may not be bounded as the theories of Houbolt and Lowson suggest. To account for the increase of static pressure through the boundary layer, Houbolt's theory can be multiplied by the $\tilde{P}_w/\bar{P}_e$ expression [Eq. (5)] to obtain (for air)

$$\frac{\tilde{P}_w}{\bar{P}_e} = \frac{M_e^2\,(0.0049 + 0.2964 \times 10^{-5}\, M_e^2)}{1 + 0.012\, M_e^2} \quad (6)$$

This modified form of Houbolt's theory is presented in Fig. 12 along with a similar modified form of Lowson's theory. As shown in the figure, $\tilde{P}_w/\bar{P}_e$ can become large at high Mach number and deviate significantly from the original form of Houbolt's and Lowson's theories.

IV. Conclusions

Extensive boundary-layer Pitot surveys, including hot-wire and preliminary wall pressure fluctuation and static pressure measurements, were obtained in helium at a nominal Mach number of 20 on the wall of a contoured nozzle with $T_w/T_{t,\infty} \approx 1.0$. The following conclusions can be made.

1) The boundary layer varied from nearly laminar to fully turbulent for the test range of Re/in. from 0.051 to 1.41×10^6 (Re_θ from 0.084 to 0.946×10^4). Measured turbulent velocity profiles along the nozzle wall were fuller in the near-wall region than profiles predicted by a nonsimilar finite difference computation method. 2) Mass flow fluctuations as large as 50% and total temperature fluctuations of 5% (determined from conventional linearized analysis) were found to be present in the inner portion of the turbulent boundary layer. 3) Near the wall, static pressure increased rapidly to a level approximately 40% above the boundary-layer edge value. The implication is that, at high Mach number, the zero pressure gradient turbulent boundary layer may have a large normal pressure gradient which necessitates improved analyses. 4) A preliminary measurement of fluctuating rms wall pressure agreed with predictions based on data obtained at lower Mach numbers. However, the ratio of $\tilde{P}_w/\bar{P}_e$ (or $\tilde{P}_w/q$) is probably not bounded at high Mach numbers as previously predicted by theory. 5) The large mass flow and wall pressure fluctuations suggest large density fluctuations near the wall, which indicate that the density fluctuation terms probably should be considered in the Reynolds stress expansion.

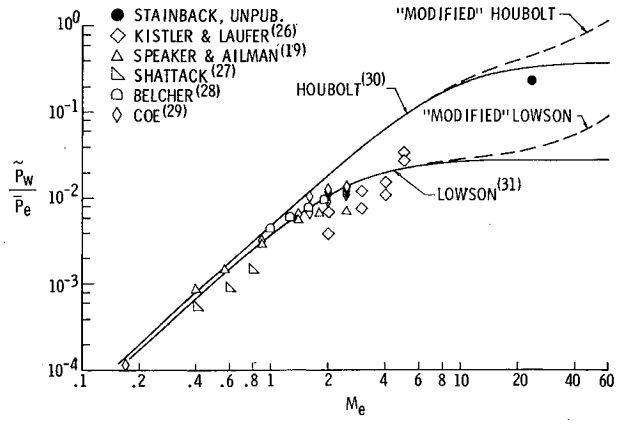

Fig. 12 Variation of rms wall pressure fluctuations with Mach number.

References

[1] Burke, A. F., "Turbulent Boundary Layers on Highly Cooled Surfaces at High Mach Numbers," Rept. 118, Nov. 1961, Cornell Aeronautical Lab., Buffalo, N.Y.

[2] Kemp, J. H., Jr. and Sreekanth, A. K., "Preliminary Results From an Experimental Investigation of Nozzle Wall Boundary Layers at Mach Numbers Ranging From 27 to 47," AIAA Paper 69-686, San Francisco, 1969.

[3] Harvey, W. D., Bushnell, D. M., and Beckwith, I. E., "Fluctuating Properties of Turbulent Boundary Layers for Mach Numbers up to 9," TN D-5496, Oct. 1969, NASA.

[4] Arrington, J. P., Joiner, R. C., Jr., and Henderson, A., Jr., "Longitudinal Characteristics of Several Configurations at Hypersonic Mach Numbers in Conical and Contoured Nozzles," TN D-2498, 1964, NASA.

[5] Wagner,R. D., Jr. and Watson, R., "Reynolds Number Effects on the Induced Pressures of Cylindrical Bodies With Different Nose Shapes and Nose Drag Coefficients in Helium at a Mach Number of 24," TR R-182, Nov. 1963, NASA.

[6] Wagner, R. D., Jr., Maddalon, D. V., and Weinstein, L. M., "Influence of Measured Freestream Disturbances on Hypersonic Boundary-Layer Transition," *AIAA Journal*, Vol. 8, No. 9, Sept. 1970, pp. 1664–1670.

[7] Kovasznay, L. S. G., "The Hot-Wire Anemometer in Supersonic Flow," *Journal of the Aeronautical Sciences*, Vol. 17, No. 9, Sept. 1950, pp. 565–572.

[8] Erickson, W. D., "Real-Gas Correction Factors for Hypersonic Flow Parameters in Helium," TN D-462, Sept. 1960, NASA.

[9] Rogers, K. W., Wainwright, J. B., and Touryan, K. J., "Impact and Static Pressure Measurements in High Speed Flows With Transitional Knudsen Numbers," *Rarefied Gas Dynamics, Proceedings of the Fourth International Symposium*, Vol. 2, Academic Press, New York, 1966, pp. 151–174.

[10] Beckwith, I. E. and Cohen, N. B., "Application of Similar Solutions to Calculation of Laminar Heat Transfer on Bodies With Yaw and Large Pressure Gradient in High-Speed Flow," TN D-625, 1960, NASA.

[11] Bushnell, D. M. and Beckwith, I. E., "Calculation of Nonequilibrium Hypersonic Turbulent Boundary Layers and Comparisons With Experimental Data," *AIAA Journal*, Vol. 8, No. 8, Aug. 1970, pp. 1462–1469.

[12] Herring, H. J. and Mellor, G. L., "A Method of Calculating Compressible Turbulent Boundary Layers," CR-1144, Sept. 1968, NASA.

[13] Wallace, J. E., "Hypersonic Turbulent Boundary-Layer

Measurements Using an Electron Beam," CAL Rept. AN-2112-Y-1, Aug. 1968, Cornell Aeronautical Lab.

[14] Laufer, J., "Some Statistical Properties of the Pressure Field Radiated by a Turbulent Boundary Layer," *The Physics of Fluids*, Vol. 7, No. 8, Aug. 1964.

[15] Kistler, A. L., "Fluctuation Measurements in a Supersonic Turbulent Boundary Layer," *The Physics of Fluids*, Vol. 2, No. 3, May–June 1959, pp. 290–296.

[16] Shaw, R., "The Influence of Hole Dimensions on Static Pressure Measurements," *Journal of Fluid Mechanics*, Vol. 7, 1960, pp. 550–564.

[17] Rainbird, W. J., "Errors in Measurement of Mean Static Pressure of a Moving Fluid Due to Pressure Holes," *Quarterly Bulletin 3*, 1967, National Research Council of Canada, National Aeronautical Establishment, pp. 55–89.

[18] Scaggs, N. E., "Boundary Layer Profile Measurements in Hypersonic Nozzles," Rept. 66-0141, July 1966, Aerospace Research Lab., U. S. Air Force.

[19] Speaker, W. V. and Ailman, C. M., "Spectra and Space-Time Correlations of the Fluctuating Pressures at a Wall Beneath a Supersonic Turbulent Boundary Layer Perturbed by Steps and Shock Waves," CR-486, May 1966, NASA.

[20] Coles, D., "Measurements in the Boundary Layer on a Smooth Flat Plate in Supersonic Flow," thesis, May 1953, California Inst. of Technology, Pasadena, Calif.

[21] Maddalon, D. V. and Henderson, A., Jr., "Boundary-Layer Transition on Sharp Cones at Hypersonic Mach Numbers," *AIAA Journal*, Vol. 6, No. 3, March 1968, pp. 424–431.

[22] Everhart, P. E. and Hamilton, H. H., "Experimental Investigation of Boundary-Layer Transition on a Cooled 7.5° Total-Angle Cone at Mach 10," TN D-4188, Oct. 1967, NASA.

[23] Lobb, R. K., Winkler, E. M., and Persh, J., "NOL Hypersonic Tunnel No. 4 Results VII: Experimental Investigation of Turbulent Boundary Layers in Hypersonic Flow," Rept. 3880, March 1955, Naval Ordnance Lab., China Lake, Calif.

[24] Perry, J. H. and East, R. A., "Experimental Measurements of Cold Wall Turbulent Hypersonic Boundary Layers," Aeronautics and Astronautics Rept. 275 Feb. 1968, Univ. of Southampton.

[25] Lowson, M. V., "Pressure Fluctuations in Turbulent Boundary Layers," TN D-3156, Dec. 1965, NASA.

[26] Richards, E. J., Bull, M. K., and Willis, J. L., "Boundary Layer Noise Research in the U.S.A. and Canada—A Critical Review," Rept. 21, 766, Feb. 1960, Aeronautical Research Council.

[27] Shattuck, R. D., "Sound Pressures and Correlations of Noise on the Fuselage of a Jet Aircraft in Flight," TN D-1086, Aug. 1961, NASA.

[28] Belcher, P. M., "Predictions of Boundary-Layer Turbulence Spectra and Correlations for Supersonic Flight," presented at the Fifth International Acoustical Congress, Liege, Belgium, Sept. 1965.

[29] Coe, C. F., "Surface-Pressure Fluctuations Associated With Aerodynamic Noise," *Conference on Basic Aerodynamic Noise Research*, NASA SP-207, July 1969, pp. 409–424.

[30] Houbolt, J. D., "On the Estimation of Pressure Fluctuations in Boundary Layers and Wakes," Rept. 90, June 1966, Aeronautical Research Association of Princeton Inc. Princeton N.J.

[31] Pierce, H. B. and Mayes, W. H., "Description of Hypersonic Boundary-Layer Noise Flight Measurement Program," *Conference on Basic Aerodynamic Noise Research*, NASA SP-207, July 1969, pp. 337–343.

MAY 1971 AIAA JOURNAL VOL. 9, NO. 5

Generalized Aerodynamic Forces on a Flexible Plate Undergoing Transient Motion in a Shear Flow with an Application to Panel Flutter

E. H. Dowell*
Princeton University, Princeton, N. J.

A theoretical solution to the title problem is obtained. Unlike previous solutions in the literature, the present method allows for finite plate dimensions and continuously varying mean velocity and temperature profiles. A computer program has been developed to calculate the required aerodynamic forces for boundary-layer profiles. These forces are then employed in a nonlinear flutter analysis previously developed by the author. The theoretical flutter results are compared with the experimental data of Muhlstein, Gaspers, and Riddle and generally good agreement is obtained. Other physical problems to which the present aerodynamic analysis is relevant include, 1) stabilization of viscous boundary layers by flexible walls, 2) sound wave propagation through shear layers, and 3) shear layer effects on control surface aerodynamics at supersonic speeds.

Nomenclature

a = plate length, also speed of sound
b = plate width
c_p, c_v = specific heats
D = plate stiffness, also derivative operator
E = modulus of elasticity
$H_{mnpq}, I_{mnpq}, K_{mnpq}$ = aerodynamic influence functions
h = plate thickness
k = reduced frequency
K = $\omega[\rho_m(ha^4/D)]^{1/2}$; also aerodynamic kernel
M = Mach number
p = pressure
Q_{mnpq} = generalized aerodynamic force
q = $\rho_\infty U_\infty^2/2$ = dynamic pressure
R = $c_P - c_v$ = gas constant
T = temperature
t = time
u,v,w = fluid velocity components
U_∞ = air velocity
w_p = plate deflection
x,y,z = spatial variables, nondimensionalized by a (or b)
z_w = wall position, nondimensionalized by a
λ^* $\equiv (2qa^3/D)$ = nondimensional dynamic pressure
μ = $\rho_\infty\theta/\rho_m h$ = mass ratio
δ = boundary-layer thickness

Received October 26, 1970; revision received February 1, 1971. Work supported by NASA Grants NGR 31-001-146 and NGR 31-001-197.

* Associate Professor, Department of Aerospace and Mechanical Sciences. Member AIAA.